The Journal of Immunology

Prevention of Vγ9Vδ2 T Cell Activation by a Vγ9Vδ2 TCR Nanobody

Renée C. G. de Bruin, Anita G. M. Stam, Anna Vangone, Paul M. P. van Bergen en Henegouwen, Henk M. W. Verheul, Zsolt Sebestyén, Jürgen Kuball, Alexandre M. J. J. Bonvin, Tanja D. de Gruijl and Hans J. van der Vliet

J Immunol 2017; 198:308-317; Prepublished online 28 November 2016;
doi: 10.4049/jimmunol.1600948
http://www.jimmunol.org/content/198/1/308

The Journal of Immunology is published twice each month by The American Association of Immunologists, Inc., 9650 Rockville Pike, Bethesda, MD 20814-3994.

Print ISSN: 0022-1767 Online ISSN: 1550-6606.

Prevention of Vγ9Vδ2 T Cell Activation by a Vγ9Vδ2 TCR Nanobody

Renée C. G. de Bruin,* Anita G. M. Stam,* Anna Vangone,[†] Paul M. P. van Bergen en Henegouwen,[‡] Henk M. W. Verheul,* Zsolt Sebestyén,[§] Jürgen Kuball,[§] Alexandre M. J. J. Bonvin,[†] Tanja D. de Gruijl,* and Hans J. van der Vliet*

Vγ9Vδ2 T cell activation plays an important role in antitumor and antimicrobial immune responses. However, there are conditions in which Vγ9Vδ2 T cell activation can be considered inappropriate for the host. Patients treated with aminobisphosphonates for hypercalcemia or metastatic bone disease often present with a debilitating acute phase response as a result of Vγ9Vδ2 T cell activation. To date, no agents are available that can clinically inhibit Vγ9Vδ2 T cell activation. In this study, we describe the identification of a single domain Ab fragment directed to the TCR of Vγ9Vδ2 T cells with neutralizing properties. This variable domain of an H chain–only Ab (VHH or nanobody) significantly inhibited both phosphoantigen-dependent and -independent activation of Vγ9Vδ2 T cells and, importantly, strongly reduced the production of inflammatory cytokines upon stimulation with aminobisphosphonate-treated cells. Additionally, in silico modeling suggests that the neutralizing VHH binds the same residues on the Vγ9Vδ2 TCR as the Vγ9Vδ2 T cell Ag-presenting transmembrane protein butyrophilin 3A1, providing information on critical residues involved in this interaction. The neutralizing Vγ9Vδ2 TCR VHH identified in this study might provide a novel approach to inhibit the unintentional Vγ9Vδ2 T cell activation as a consequence of aminobisphosphonate administration. ***The Journal of Immunology*, 2017, 198: 308–317.**

In human peripheral blood the predominant subset of γδ T cells consists of Vγ9Vδ2 T cells, and these cells play an important role in the defense against microbial pathogens, stressed cells, and tumor cells of various origin (1, 2). Vγ9Vδ2 T cells become activated by the MHC-independent recognition of non–peptide phosphoantigens that are produced as an intermediate product of the bacterial non–mevalonate pathway or that are upregulated upon stress or malignant transformation by the mevalonate pathway leading to cholesterol synthesis (3–5). Activated Vγ9Vδ2 T cells produce large amounts of the proinflammatory cytokines IFN-γ and TNF-α as well as the chemokines MIP-1 and RANTES. Additionally, cytolytic mediators such as granzyme B and perforin are produced to induce specific lysis of cells with elevated phosphoantigen levels (6). It has been reported that the type I membrane protein butyrophilin 3A1 (BTN3A1, also known as CD277) directly or indirectly recognizes elevated levels of intracellular phosphoantigen and as a consequence undergoes a conformational change and membrane redistribution that is sensed by the Vγ9Vδ2 TCR, most likely through an inside-out mechanism (7–9).

Although Vγ9Vδ2 T cell activation has been shown to be important in both antitumor and antimicrobial immune responses, there are conditions in which Vγ9Vδ2 T cell activation can be considered inappropriate to the host (2, 10–14). One third to half of all patients undergoing aminobisphosphonate (NBP, e.g., pamidronate and zoledronate) treatment for hypercalcemia, osteoporosis, or metastatic bone disease experience flu-like symptoms (chills, fatigue, myalgia) and elevated body temperature that resemble an acute phase response (APR) (15–17). NBP exposure leads to the inhibition of a crucial step in the mevalonate pathway resulting in a (desired) defective formation, activity, and survival of osteoclasts, but it also induces (unintended) phosphoantigen accumulation and subsequent Vγ9Vδ2 T cell activation. It has been demonstrated that the observed APR results from the cytokines produced by activated Vγ9Vδ2 T cells (18–21). Apart from being bothersome to patients, repeated NBP administration may result in Vγ9Vδ2 T cell unresponsiveness by the induction of anergy and exhaustion (22). Although this will limit the severity of the APR, it might also reduce overall antitumor and antimicrobial immunity, as this is in part controlled by a functional Vγ9Vδ2 T cell population. Efforts to dampen the APR resulting from NBP administration, for example, by coadministration of statins, have been largely unsuccessful (23–25).

A potential and novel way to block ligand binding is the application of variable domains of an H chain–only Ab (VHHs), which are variable domains of naturally occurring H chain–only Abs (also called nanobodies). These single-domain Ab fragments are characterized by a small size (∼15 kDa) and enhanced stability compared with conventional Abs. VHHs have low immunogenicity

*Department of Medical Oncology, VU University Medical Center, 1081 HV Amsterdam, the Netherlands; [†]Bijvoet Center for Biomolecular Research, Faculty of Science, Utrecht University, 3584 CH Utrecht, the Netherlands; [‡]Department of Cell Biology, Faculty of Science, Utrecht University, 3584 CH Utrecht, the Netherlands; and [§]Laboratory of Translational Immunology, Department of Hematology, University Medical Center Utrecht, 3508 GA Utrecht, the Netherlands

ORCIDs: 0000-0003-2485-7378 (A.V.); 0000-0001-6050-9042 (P.M.P.v.B.e.H.); 0000-0001-7369-1322 (A.M.J.J.B.).

Received for publication June 3, 2016. Accepted for publication November 2, 2016.

This work was supported by Dutch Cancer Society Grant VU 2010-4728 (to H.J.v.d.V.) and by Dutch Foundation for Scientific Research TOP-PUNT Grant 718.015.001 (to A.M.J.J.B.). A.V. was supported by Grant BAP-659025 from Marie Sklodowska-Curie Individual Fellowship MSCA-IF-2015. Z.S. and J.K. were supported by Worldwide Cancer Research Grants 10-0736 and 15-0049.

Address correspondence and reprint requests to Dr. Hans. J. van der Vliet, VU University Medical Center, Department of Medical Oncology, Room 3A38, De Boelelaan 1117, 1081 HV Amsterdam, the Netherlands. E-mail address: jj.vandervliet@vumc.nl

The online version of this article contains supplemental material.

Abbreviations used in this article: 7-AAD, 7-aminoactinomycin D; APR, acute phase response; BTN3A1, butyrophilin 3A1; CLL, chronic lymphocytic leukemia; IPP, isopentenyl pyrophosphate; NBP, aminobisphosphonate; PDB, Protein Data Bank; VHH, variable domain of an H chain–only Ab.

www.jimmunol.org/cgi/doi/10.4049/jimmunol.1600948

and can be produced by bacteria or yeast, allowing time and cost reduction in the manufacturing process (26–28). Ligand blocking has successfully been demonstrated for anti–epidermal growth factor receptor VHHs that could block binding of epidermal growth factor to its receptor (29). Previously, we have successfully generated a novel set of 20 VHHs directed to the Vγ9 and/or Vδ2 chain of the Vγ9Vδ2 TCR that can be used for flow cytometry, immunocytochemistry, and magnetic cell purification (30). In this study, we evaluate whether these VHHs could be developed for future therapeutic manipulation of Vγ9Vδ2 T cells. We report that a Vδ2 chain–specific VHH can inhibit both phosphoantigen-dependent and -independent BTN3A1-restricted stimulation of Vγ9Vδ2 T cells, resulting in a strong reduction of cytokine secretion. In silico modeling predicted this VHH to dock and interact with a region on the Vγ9Vδ2 TCR that has been implicated in phosphoantigen/BTN3A1-mediated Vγ9Vδ2 T cell activation. As this Vγ9Vδ2 TCR–specific VHH blocked NBP-induced Vγ9Vδ2 T cell activation in peripheral blood as well as spontaneous and NBP-induced activation of Vγ9Vδ2 T cells by lymphoma cells, this VHH could constitute an interesting novel therapeutic agent to prevent the Vγ9Vδ2 T cell–induced APR in NBP-treated patients.

Materials and Methods

Cell lines

HeLa cells were obtained from the American Type Culture Collection and cultured in DMEM complete media, that is, DMEM (Lonza, catalog no. BE12-614F) supplemented with 10% (v/v) heat-inactivated FCS (HyClone; GE Healthcare, catalog no. SV30160.03), 100 IU/ml sodium penicillin, 100 μg/ml streptomycin sulfate, and 2.0 mM L-glutamine (Life Technologies, catalog no. 10378-016). Jurma cells were transduced to express wild-type Vγ9Vδ2 TCR G115 or indicated δ2 G115 CDR3 mutants as described previously (10) and cultured in RPMI complete media, that is, RPMI 1640 medium (Lonza, catalog no. 5MB048) supplemented with 10% (v/v) heat-inactivated FCS, 0.05 mM 2-ME, 100 IU/ml sodium penicillin, 100 μg/ml streptomycin sulfate, and 2.0 mM L-glutamine. Burkitt's lymphoma Daudi cells were obtained from the American Type Culture Collection and cultured in RPMI complete media. FCS was from a single lot previously tested for low background. The cell lines were maintained at 37°C with 5% CO_2 in a humidified atmosphere and tested mycoplasma negative.

Generation of donor-derived γδ T cells

Healthy donor Vγ9Vδ2 T cells were isolated, expanded, and cultured from heparinized whole blood as described (31). In short, Vγ9Vδ2 T cells were isolated from PBMCs using FITC-labeled anti-TCR Vδ2 or PE-labeled anti-TCR Vγ9 mAbs in combination with anti-mouse IgG MicroBeads (Miltenyi Biotec, catalog no. 130-048-401) by MACS. Purified Vγ9Vδ2 T cells were stimulated once a week with irradiated and NBP-treated (100 μM pamidronate for 3 h; Teva Pharmachemie, catalog no. 12J08RD) human mature monocyte-derived dendritic cells or an irradiated feeder mixture (PBMCs of two healthy human donors and EBV-transformed B cells with addition of 50 ng/ml PHA). Vγ9Vδ2 T cells were only used for experiments when cell viability determined by trypan blue staining was >70%, $V\gamma9^+V\delta2^+$ TCR expression determined by flow cytometry was >90%, and CD25 expression was <40%.

$V\gamma9^-V\delta2^+$, $V\gamma9^+V\delta2^-$, $V\gamma9^+V\delta2^+$, and $V\gamma9^-V\delta2^-$ γδ T cell lines for the determination of VHH specificity were generated as follows. A pan-γδ T cell population was isolated from human PBMCs using a PE-labeled pan-γδ TCR Ab and purified with MACS using anti-mouse IgG MicroBeads. The pan-γδ T cell line was first expanded with feeder mixture and then sorted into four separate populations (i.e., $V\gamma9^-V\delta2^+$, $V\gamma9^+V\delta2^-$, $V\gamma9^+V\delta2^+$, and $V\gamma9^-V\delta2^-$ γδ T cells) by flow cytometric cell sorting using FITC-labeled anti-TCR Vδ2 and PE-labeled anti-TCR Vγ9 mAbs.

All donor-derived Vγ9Vδ2 T cell lines were cultured in Yssel's medium (32) supplemented with 1% heat-inactivated human AB serum (Cellect; MP Biomedicals, catalog no. 2931949), 50 U/ml recombinant human IL-2 (Proleukin; Novartis), 0.05 mM 2-ME, 100 IU/ml sodium penicillin, 100 μg/ml streptomycin sulfate, and 2.0 mM L-glutamine. During experiments, Vγ9Vδ2 T cell lines and target cell lines were cultured in IMDM complete media medium, that is, IMDM (Lonza, catalog no. BE12-722F) supplemented with 10% (v/v) FCS, 0.05 mM 2-ME, 100 IU/ml sodium penicillin, 100 μg/ml streptomycin sulfate, and 2.0 mM L-glutamine. Human AB serum was from a single lot previously tested for low background and viable and responsive Vγ9Vδ2 T cell cultures. The Vγ9Vδ2 T cell lines were maintained at 37°C with 5% CO_2 in a humidified atmosphere and tested mycoplasma negative.

Generation of Vγ9Vδ2 TCR– and Vα24Vβ11 TCR–transduced cell lines

Jurkat cells transduced to express TCRs of interest were generated as described previously (33). For the Vγ9Vδ2 TCR, protein sequences of clone G9 Vγ9 and Vδ2 chain (34, 35) were used. For the Vα24Vβ11 TCR, protein sequences of clone NKT12 Vα24 and Vβ11 chain (36) were used. Sequences of the individual TCR chains were separated by a picorna virus–derived 2A sequence, codon modified for optimal protein production, and synthesized by GeneART (Thermo Fisher Scientific, Waltham, MA), after which they were cloned into the LZRS vector. After transfection to the Phoenix-A packaging cell line, retroviral supernatants were collected to transduce Jurkat cells in the presence of retronectin (Takara Bio, catalog no. T100A) according to the manufacturer's protocol (33). The transduced cell lines were purified for TCR expression by MACS cell separation with anti-mouse IgG MicroBeads or by flow cytometric sorting using FITC-labeled anti-TCR Vδ2 and PE-labeled anti-TCR Vγ9 mAbs or FITC-labeled anti-TCR Vα24 and PE-labeled anti-TCR Vβ11 mAbs as appropriate.

Production and purification of VHH

VHH DNA from individual clones was cloned into plasmid pMEK219 (a gift of Mohamed El Khattabi, QVQ, Utrecht, the Netherlands), a derivative from pHen1 (37) with addition of an HC-V cassette to enable VHH cloning, a C-terminal Myc- and 6× His-tag, and deletion of the gene III sequence. TG1 bacteria were transformed with pMEK219-VHH for protein production. Bacteria were inoculated in 2xYT (Serva, catalog no. 48501.01) plus 100 μg/ml ampicillin and 0.1% glucose and grown to log phase, and protein production was induced by addition of a final concentration of 1 mM isopropyl β-D-thiogalactoside (Thermo Fisher Scientific, catalog no. R0391). VHHs were released from the bacterial periplasm by a PBS freeze-thawing step and purified by immobilized metal ion affinity chromatography on TALON resin (Clontech, catalog no. 635504). VHHs were eluted with 150 mM imidazole and dialyzed twice against PBS. The purity of the VHHs was checked by Coomassie-stained protein gel.

Flow cytometry and mAbs

mAbs used were FITC-labeled anti-TCR Vδ2 (catalog no. 555738), FITC-labeled anti-CD69 (catalog no. 347823), PE-labeled anti-CD107a (catalog no. 555801), PE-labeled anti-CD25 (catalog no. 55542), allophycocyanin-labeled anti-CD25 (catalog no. 340907), and 7-aminoactinomycin D (7-AAD; catalog no. 559925) from BD Biosciences. PerCP-labeled anti-TCR Vδ2 (catalog no. 331410), PE-labeled anti-TCR Vγ9 (catalog no. 331308), and allophycocyanin-labeled anti-TCR Vγ9 (catalog no. 331310) were from BioLegend. RPE–labeled goat anti-mouse $F(ab')_2$ fragment (catalog no. R0480) was obtained from Dako, and allophycocyanin-labeled goat anti-mouse $F(ab')_2$ fragment (catalog no. SC-3818) was obtained from Santa Cruz Biotechnology. Anti-Myc tag mAb clone 4A6 (catalog no. 05-724) was obtained from Merck Millipore.

All stainings for flow cytometry were performed in PBS supplemented with 0.1% BSA and 0.02% sodium azide. Stained cells were directly analyzed by flow cytometry. All samples of individual experiments for the same figures were either measured with FACSCalibur or LSRFortessa (both BD Biosciences). Photomultiplier tube voltages for FACSCalibur were set with unstained control cells, and for LSRFortessa the settings of the manufacturer were used. Data were analyzed with CellQuest (BD Biosciences) or Kaluza software (Beckman Coulter). The generated data can be provided per request.

Functional analyses of inhibition of Vγ9Vδ2 T cell activation by VHH 5E7

Human healthy donor-derived PBMCs or Vγ9Vδ2 T cells were incubated for 1 h with 0–500 nM VHH in IMDM complete media at 4°C, after which they were exposed to either 1) NBP-treated PBMCs, HeLa cells, or Daudi cells that were cultured for 2 h with 0–100 μM pamidronate in IMDM complete media at 37°C for 2 h, washed with PBS three times, and resuspended in IMDM complete media; 2) Daudi cells that were cultured overnight with 12.5 μM mevastatin (Sigma-Aldrich, catalog no. M2537) in culture medium, washed, and resuspended in IMDM complete media; or 3)

PBMCs cultured with 0 or 20 μM anti-BTN3A1 mAb (eBioscience, catalog 14-2779-82) for 1 h at 4°C followed by incubation for 1 additional hour at 37°C, washed with PBS, and resuspended in IMDM complete media.

For the 1:1 cocultures of Vγ9Vδ2 T cells with target cells, 5×10^4 Vγ9Vδ2 T cells were cultured together with 5×10^4 Daudi or HeLa cells for 4 or 24 h, respectively, in a final volume of 200 μl of IMDM complete media. The PBMCs were cultured for 24 h in IMDM complete media. For HeLa cell cocultures, culture supernatants were collected after 20 h to determine IFN-γ and TNF-α by ELISA (PeliKine compact ELISA kits; Sanquin, catalog nos. M1933 and M9323, respectively) according to the manufacturer's instructions. To determine the expression of CD107a, anti-CD107a mAb and GolgiStop (BD Biosciences, catalog no. 554724) were added during the final 4 h of the experiment. At the end of the experiment, cells were stained with 7-AAD (according to the manufacturer's protocol), anti-CD25 mAb, or anti-CD69 mAb and analyzed by flow cytometry.

Binding analysis of VHH 5E7 to γδ TCR–expressing cells in FACS

To determine the binding of VHH 5E7 to donor-derived γδ T cells or (TCR-transduced) Jurkat cells, 5×10^4 cells were incubated with 100 nM VHH for 30 min. Bound VHH was detected with anti–Myc-tag mAb clone 4A6 and allophycocyanin- or RPE-labeled goat-anti-mouse $F(ab')_2$ fragment by flow cytometry.

To determine the binding persistence and stability of VHH 5E7 to Vγ9Vδ2 T cells, Vγ9Vδ2 T cells were incubated with 100 nM VHH, cultured for 0, 8, or 15 d in Yssel's medium (32) supplemented with 1% AB human serum, 0.05 mM 2-ME VHH and, 100 IU/ml sodium penicillin, 100 μg/ml streptomycin sulfate, 2.0 mM L-glutamine, and 10% human serum albumin (Sigma-Aldrich, catalog no. A9731). A final concentration of 10 U/ml recombinant human IL-2 (Proleukin; Novartis) was added to the culture every 3 d. On days 0, 8, and 15 a sample was taken from the culture and VHH bound to the Vγ9Vδ2 T cells was detected with anti–Myc-tag mAb clone 4A6 and allophycocyanin- or RPE-labeled goat anti-mouse $F(ab')_2$ fragment by flow cytometry.

Statistical analyses of biological experiments

Statistical analyses were performed with GraphPad Prism version 5 (GraphPad Software, La Jolla, CA) using a one-way or two-way ANOVA with a Bonferroni post hoc test as appropriate. Findings were considered significant when p values were <0.05.

Homology modeling of VHH 5E7

Starting from the sequence of VHH 5E7, we modeled its three-dimensional structure by homology modeling. A BLASTp (38) search with default parameters was performed against the Protein Data Bank (PDB) (39) to find a suitable template for homology modeling. Among the templates specifically showing the same length for the three CDRs of our query, we chose the one with highest sequence identity: PDB code 4KRN (chain A, 78% of sequence identity, 1.55 Å of resolution) (40). This template was used for homology modeling using Modeler v9.10 (41). The top five homology models according to the dope score (42) were selected for the docking.

Modeling of the Vγ9Vδ2 TCR–VHH 5E7 and Vγ9Vδ2 TCR–BTN3A1 complexes

To identify the Vγ9Vδ2 TCR regions involved in the binding with VHH 5E7 and BTN3A1, we performed docking simulations of the Vγ9Vδ2 TCR–VHH 5E7 and Vγ9Vδ2 TCR–BTN3A1 complexes using HADDOCK (43–45). HADDOCK is a high ambiguity–driven docking program making use of biochemical and/or biophysical interaction data (translated into ambiguous interaction restraints) to drive docking. It makes use of a crystallographic and NMR system (46) as its structure calculation engine. The protocol consists of three steps: 1) randomization of orientation and rigid body docking by energy minimization driven by interaction restraints (it0), 2) semiflexible refinement in torsion angle space in which side chains and backbone atoms of the interface residues are allowed to move (it1), and 3) Cartesian dynamics refinement in explicit solvent. The final models are clustered using the pairwise backbone root mean square deviation at the interface. The resulting clusters are analyzed and ranked according to the HADDOCK score, a weighted sum of van der Waals, electrostatic, empirical desolvation (47), and restraint violation energies. As input structures for the Vγ9Vδ2 TCR and BTN3A1, we used the available experimental structures with PDB code 1HXM (chains A and B) (34) and 4F9L (chain A) (7), respectively. In both cases, we first refined the structures using the final water refinement stage of HADDOCK. The ensemble of the top five refined structures was then used as input for the docking runs for both Vγ9Vδ2 TCR and BTN3A1. For the VHH 5E7, we used an ensemble of the top five homology models as input (see above).

Docking runs. Given the lack of experimental information on the interactions between these proteins, we first ran ab initio docking between Vγ9Vδ2 TCR and VHH 5E7 with center of mass restraints, which effectively brings the molecules in contact by specifying a distance restraint between their respective centers of mass. All 10,000 rigid-body docking models (it0-run1) (first stage of HADDOCK) were analyzed to identify the top 10% contacted residues (see below) on each protein. This information was used in a second docking run (it0-run2) to refine the binding surface on VHH 5E7, and all of the residues of the Vγ9Vδ2 TCR with >40% relative solvent-accessible area were defined as passive (excluding the transmembrane residues). Finally, to further pinpoint the binding site on the Vγ9Vδ2 TCR, a third run was performed with the most contacted residues on both VHH 5E7 and the Vγ9Vδ2 TCR defined as active. The active residues for the Vγ9Vδ2 TCR were obtained from an analysis of the most contacted residues in it0-run2. All runs were performed with default parameters, except for more models (10,000, 400, and 400 for it0, it1, and water refinement, respectively).

The same procedure was applied for the docking of the systems composed by the Vγ9Vδ2 TCR–BTN3A1.

A complete list of the restraints for each run is provided in Supplemental Table I. The analysis of the most contacted residues was performed through the CONS-COCOMAPS server (48). Solvent-accessible surface area was calculated using Naccess (http://www.bioinf.manchester.ac.uk/naccess).

Results

Identification and characterization of neutralizing Vγ9Vδ2 TCR–specific VHHs

To generate neutralizing Vγ9Vδ2 TCR VHHs, two llamas (*Lama glama*) were s.c. injected with 10^8 purified human healthy donor-derived Vγ9Vδ2 T cells for four times during a period of 6 wk. Using phage display selections, a panel of 20 distinct Vγ9Vδ2 TCR–specific monoclonal VHHs was obtained from the llama immune libraries. From this, the VHH with the best Vγ9Vδ2 TCR neutralizing properties was VHH clone 5E7. Vγ9Vδ2 TCR specificity of VHH 5E7 was confirmed by binding assays using different TCR-expressing cell lines. VHH 5E7 was allowed to bind to a Jurkat cell line genetically modified to express the Vγ9Vδ2 TCR (Jurkat Vγ9Vδ2 TCR). As negative controls, a Jurkat cell line without TCR expression and a Jurkat cell line transduced to express an αβ TCR were used. VHH 5E7 bound to Jurkat Vγ9Vδ2 TCR cells but not to the control Jurkat cell lines, indicating specificity for the Vγ9Vδ2 TCR but not for the αβ TCR or CD3 coexpressed in the TCR complex (Fig. 1A). Additionally, VHH 5E7 demonstrated strong binding to healthy donor-derived Vγ9Vδ2 T cells, and not to $V\gamma9^-V\delta2^-$ γδ T cells (Fig. 1B), confirming the specificity of Vγ9Vδ2 TCR binding by VHH 5E7.

The capacity of VHH 5E7 to inhibit Vγ9Vδ2 T cell activation was studied by coculturing healthy donor–derived Vγ9Vδ2 T cells with NBP-treated HeLa cells in a 1:1 ratio for 24 h in the presence or absence of the VHH or a nonspecific control VHH. Vγ9Vδ2 T cell activation was assessed by determining CD25 upregulation by flow cytometry. VHH 5E7 could significantly inhibit phosphoantigen-mediated Vγ9Vδ2 T cell activation in multiple donors in a dose-dependent manner (Fig. 2A). Importantly, the nonspecific control VHH did not inhibit Vγ9Vδ2 T cell activation nor did VHH 5E7 significantly influence CD25 expression of Vγ9Vδ2 T cells when cells were not treated with NBP.

Next, we analyzed whether this VHH was capable of inhibiting Vγ9Vδ2 T cell cytokine production and degranulation upon target cell recognition. For this purpose, IFN-γ and TNF-α were selected as prototypic cytokines known to be produced by activated Vγ9Vδ2 T cells. Indeed, in culture supernatants obtained after a 24 h coculture of Vγ9Vδ2 T cells with NBP-treated HeLa cells, VHH 5E7 was found to significantly inhibit the production of both

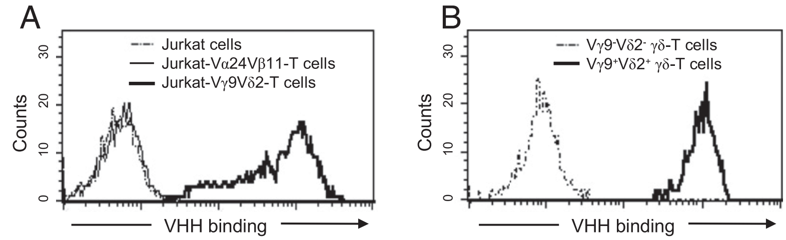

FIGURE 1. VHH 5E7 specifically binds the Vγ9Vδ2 TCR. (**A**) VHH 5E7 binds to Jurkat Vγ9Vδ2 TCR cells (thick line), but not to Jurkat cells without TCR expression (striped line) or Jurkat Vα24Vβ11 TCR cells (thin line). (**B**) VHH 5E7 binds to healthy donor-derived $V\gamma9^{+}V\delta2^{+}$ γδ T cells (thick line), but not to $V\gamma9^{-}V\delta2^{-}$ γδ T cells (striped line). (A and B) VHH binding was determined by flow cytometry. A representative figure is shown of $n = 3$ experiments (biological replicates).

IFN-γ and TNF-α in a dose-dependent fashion (Fig. 2B, 2C). As expected, the nonspecific control VHH did not inhibit the production of IFN-γ and TNF-α by NBP-activated Vγ9Vδ2 T cells. Degranulation of Vγ9Vδ2 T cells, as a measure for cytotoxic activity, was determined by assessing cell surface expression of the lysosomal-associated membrane protein-1 (CD107a) by Vγ9Vδ2 T cells in response to target cell recognition. In line with the previous experiments, and in contrast to the nonspecific control VHH, VHH 5E7 was found to dose-dependently and significantly block CD107a translocation in Vγ9Vδ2 T cells when cocultured with NBP-treated HeLa cells (Fig. 2D). To confirm that the inhibition of Vγ9Vδ2 T cell activation and degranulation was accompanied by reduced target cell lysis, we determined lysis of NBP-treated HeLa cells after a 24 h coculture with Vγ9Vδ2 T cells in the presence or absence of VHH 5E7 or the nonspecific control VHH and found that VHH 5E7 indeed significantly reduced the lysis of target cells by 38 ± 10% (mean ± SEM) whereas the nonspecific VHH did not (Fig. 2E). Activation, cytokine production, degranulation, and cytotoxicity of Vγ9Vδ2 T cells are the result of functional signaling upon the accumulation of tyrosine-phosphorylated proteins close to the immunological synapse as a consequence of Vγ9Vδ2 T cell stimulation by phosphoantigen (49). Because these processes are inhibited by VHH 5E7, it is likely that VHH 5E7 inhibits the formation of immunological synapses between Vγ9Vδ2 T cells and target cells. This is supported by our observation that VHH 5E7, but not a nonspecific control VHH, dose-dependently inhibited trogocytosis, an active, rapid, and polarized bidirectional exchange of membrane patches in the immunological synapse that forms between immune effector and target cells (50–53), that is, between Vγ9Vδ2 T cells and phosphoantigen-expressing target cells (Supplemental Fig. 1).

To further characterize the Vγ9Vδ2 TCR–specific VHH 5E7, we determined its binding affinity and stability over time. For an assessment of binding affinity, Jurkat Vγ9Vδ2 TCR cells were incubated with different concentrations of VHH 5E7 to determine the concentration at which half of the maximum fluorescence intensity was reached by flow cytometry analysis. This revealed that VHH 5E7 had an affinity of ~2.3 nM (data not shown). Next,

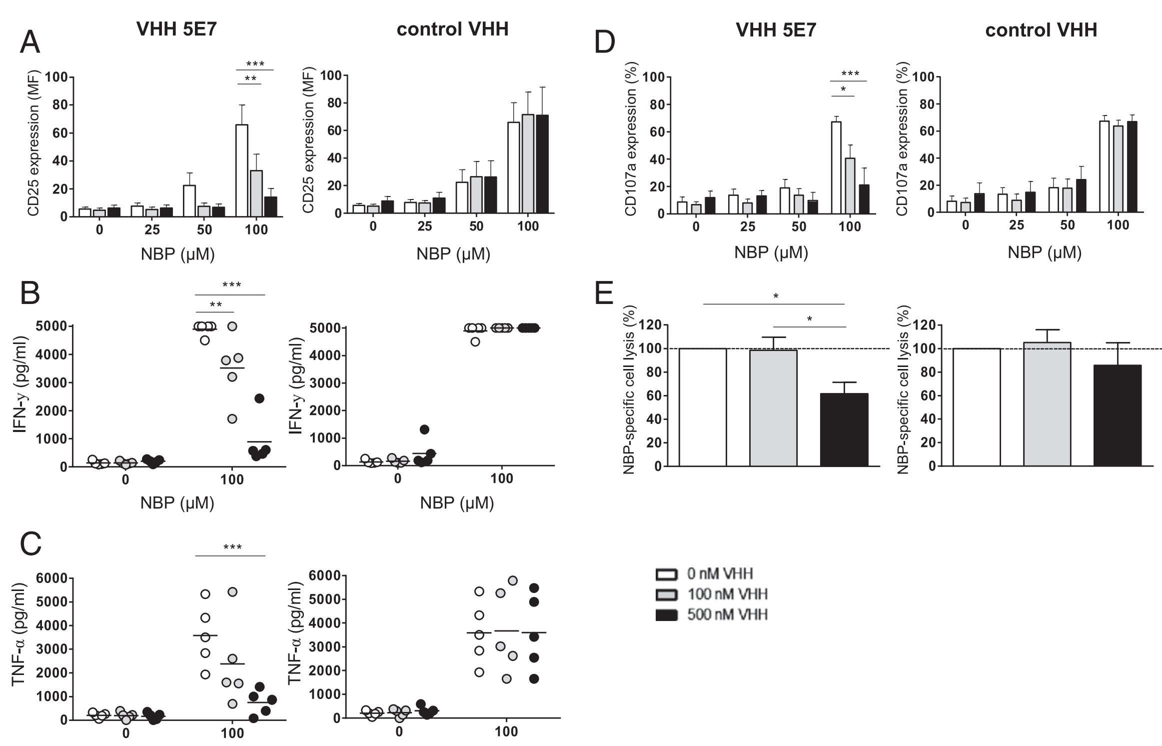

FIGURE 2. Vγ9Vδ2 T cell activation by NBP-treated cells can be inhibited by a Vγ9Vδ2 TCR–specific VHH. VHH 5E7 (left panels) but not a nonspecific control VHH (right panels) inhibits Vγ9Vδ2 T cell activation. Vγ9Vδ2 T cells were cocultured without VHH (white), with 100 nM VHH (gray), or with 500 nM VHH (black) and NBP-treated HeLa cells in a 1:1 ratio. (**A**–**D**) Activation of Vγ9Vδ2 T cells was assessed by upregulation of activation markers and secreted cytokine levels in the culture medium. (A) CD25 expression on Vγ9Vδ2 T cells assessed by flow cytometry. (B and C) IFN-γ secretion (B) and TNF-α secretion (C) by Vγ9Vδ2 T cells as determined by ELISA. (D) CD107a expression on Vγ9Vδ2 T cells assessed by flow cytometry. (**E**) NBP-specific lysis of HeLa cells. The percentage of lysed HeLa cells ($7\text{-}AAD^{+}$) was determined by flow cytometry. VHH conditions (0 nM) were set to 100%. (A–E) Shown are means ± SEM of at least $n = 3$ experiments (biological replicates). The p values were calculated with a two-way ANOVA and a Bonferroni post hoc test. $*p < 0.05$, $**p < 0.01$, $***p < 0.001$. MF, mean fluorescence intensity.

we analyzed how long after exposure VHH 5E7 could still be detected on the surface of Vγ9Vδ2 T cells when cultured at 37°C in the presence of 10% human serum albumin. Even at day 15, VHH 5E7 was still detectable on all Vγ9Vδ2 T cells, underscoring its high target affinity and stability (Fig. 3). As was to be expected by natural downregulation and degradation of expressed Vγ9Vδ2 TCRs and the synthesis and expression of new Vγ9Vδ2 TCRs over time, the amount of VHH bound per Vγ9Vδ2 T cell, as reflected by mean fluorescence intensity, did decrease over time. In conclusion, from our panel of 20 VHHs, we selected VHH 5E7 as the most potent inhibitor of NBP-mediated Vγ9Vδ2 T cell activation.

Vγ9Vδ2 TCR–specific VHH 5E7 inhibits BTN3A1 mAb-mediated activation of Vγ9Vδ2 T cells

In addition to NBP-mediated activation, Vγ9Vδ2 T cells have previously also been shown to become activated by target cells treated with the agonistic anti-BTN3A1 mAb 20.1 in a phosphoantigen-independent manner (54). To investigate the mechanism underlying BTN3A1-induced Vγ9Vδ2 T cell activation, we determined whether VHH 5E7 was capable of inhibiting the phosphoantigen-independent mode of Vγ9Vδ2 T cell activation. To this end, PBMCs were cultured with the agonistic anti-BTN3A1 mAb 20.1 in the presence or absence of VHH 5E7. After 24 h, Vγ9Vδ2 T cell activation was assessed by upregulation of CD25 and CD69 on Vγ9Vδ2 T cells by flow cytometry. Vγ9Vδ2 T cells could be activated by the anti-BTN3A1 mAb 20.1, and this effect was significantly and specifically blocked by the addition of VHH 5E7 (as shown in Fig. 4). In conclusion, the Vγ9Vδ2 TCR–specific VHH 5E7 inhibited Vγ9Vδ2 T cell activation induced by phosphoantigen-overexpressing target cells as well as by target cells treated with the BTN3A1-specific mAb 20.1.

Structural in silico analysis of the interaction between VHH 5E7 and the Vγ9Vδ2 TCR

To explain the inhibiting effect of VHH 5E7 on both phosphoantigen-dependent and -independent activation of Vγ9Vδ2 T cells, we reasoned that VHH 5E7 could bind a crucial epitope on the Vγ9Vδ2 TCR that is required for the BTN3A1-mediated activation of Vγ9Vδ2 T cells. To further evaluate this, we first determined whether there was predominant binding of VHH 5E7 to either the Vγ9 chain or the Vδ2 chain of the Vγ9Vδ2 TCR. For this purpose, a pan-γδ T cell line (bulk culture) was generated from human PBMCs by magnetic bead isolation and subsequently separated into four distinct populations by flow cytometric sorting: $V\gamma9^-V\delta2^+$, $V\gamma9^+V\delta2^-$, $V\gamma9^+V\delta2^+$, and $V\gamma9^-V\delta2^-$ γδ T cells. VHH 5E7 showed strong binding to $V\gamma9^-V\delta2^+$ and $V\gamma9^+V\delta2^+$ γδ T cells but not to $V\gamma9^+V\delta2^-$ or $V\gamma9^-V\delta2^-$ γδ T cells (Fig. 5A), indicating that VHH 5E7 specifically requires the δ2 chain for binding. Of note, the flow cytometry–based binding analysis showed that VHH 5E7 bound the $V\gamma9^+V\delta2^+$ γδ T cell population with a higher mean fluorescence intensity than did the $V\gamma9^-V\delta2^+$ γδ T cell population, indicating that although VHH 5E7 primarily binds to the Vδ2 chain, the presence of the Vγ9 chain may stabilize this binding.

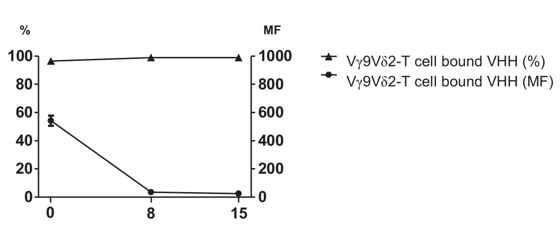

FIGURE 3. Stability of binding of VHH 5E7 to Vγ9Vδ2 T cells. Vγ9Vδ2 T cells were incubated with VHH 5E7, washed, and cultured for the indicated time periods in the presence of human serum albumin (10%). Bound VHH to Vγ9Vδ2 T cells was detected by flow cytometry directly after binding (day 0), after 8 d, and after 15 d of culturing. Both the percentage and mean fluorescence intensity (MF) of bound VHH to Vγ9Vδ2 T cells are shown. Shown are means ± SEM of $n = 3$ experiments (biological replicates).

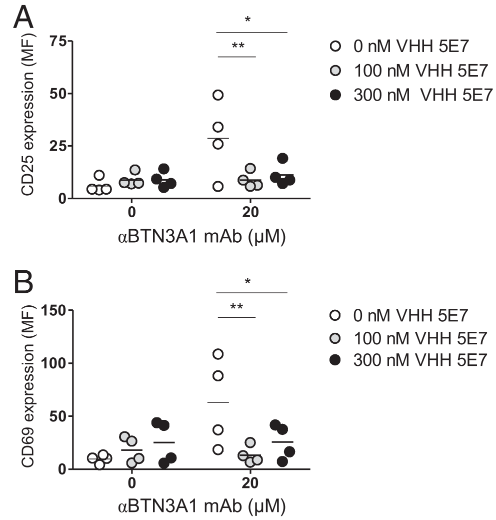

FIGURE 4. VHH 5E7 inhibits anti-BTN3A1 mAb–induced Vγ9Vδ2 T cell activation. PBMCs were preincubated without VHH (white), with 100 nM VHH 5E7 (gray), or with 300 nM VHH 5E7 (black) in the presence or absence of anti-BTN3A1 mAb 20.1 and cultured for 24 h. Vγ9Vδ2 T cell activation within the PBMC pool was assessed by upregulation of (**A**) CD25 or (**B**) CD69 as determined by flow cytometry. Shown are means ± SEM of $n = 4$ experiments (biological replicates). The p values were calculated with a two-way ANOVA and a Bonferroni post hoc test. $^*p < 0.05$, $^{**}p < 0.01$. MF, mean fluorescence intensity.

To identify the region of the Vγ9Vδ2 TCR interacting with VHH 5E7, we generated models of the complex of the Vγ9Vδ2 TCR with VHH 5E7 using HADDOCK (43–45). A model of VHH 5E7 was built by homology modeling as described in *Materials and Methods*, whereas the crystal structure of the Vγ9Vδ2 TCR (PDB code 1HXM) (34) was available. We first ran an ab initio docking using the "center of mass" restraints protocol in HADDOCK. From a statistical analysis of the most frequently contacted residues within the pool of generated models, no clear region emerged for the Vγ9Vδ2 TCR, although the three CDRs of the Vγ9Vδ2 TCR were found at the binding interface for VHH 5E7. Subsequently, a second docking run was performed with the CDRs of VHH 5E7 defined as "active" residues and all the solvent-exposed accessible residues of the Vγ9Vδ2 TCR as "passive" residues (excluding the transmembrane region) (see Supplemental Table I and *Materials and Methods*) to drive the docking. The in silico statistical contact analysis of the models (see *Materials and Methods*) obtained with this second run clearly revealed preferred interactions of VHH 5E7 with Vγ9Vδ2 TCR, in particular at δ2 CDR3 (Glu^{102} and Tyr^{103}), γ9 CDR1 (Ala^{32}), γ9 CDR2 (Tyr^{54} and Arg^{59}), and γ9 CDR3 (Trp^{100}, Leu^{106}, Gly^{107}, and Lys^{109}) (Table I), which is in agreement with the VHH 5E7 in vitro binding analysis performed with the different γδ T cell populations.

The exact mode of recognition between Vγ9Vδ2 T cells and BTN3A1-expressing cells has not yet been elucidated. Vavassori et al. (55) have provided evidence for a direct (low affinity) interaction between BTN3A1 and the Vγ9Vδ2 TCR. To study

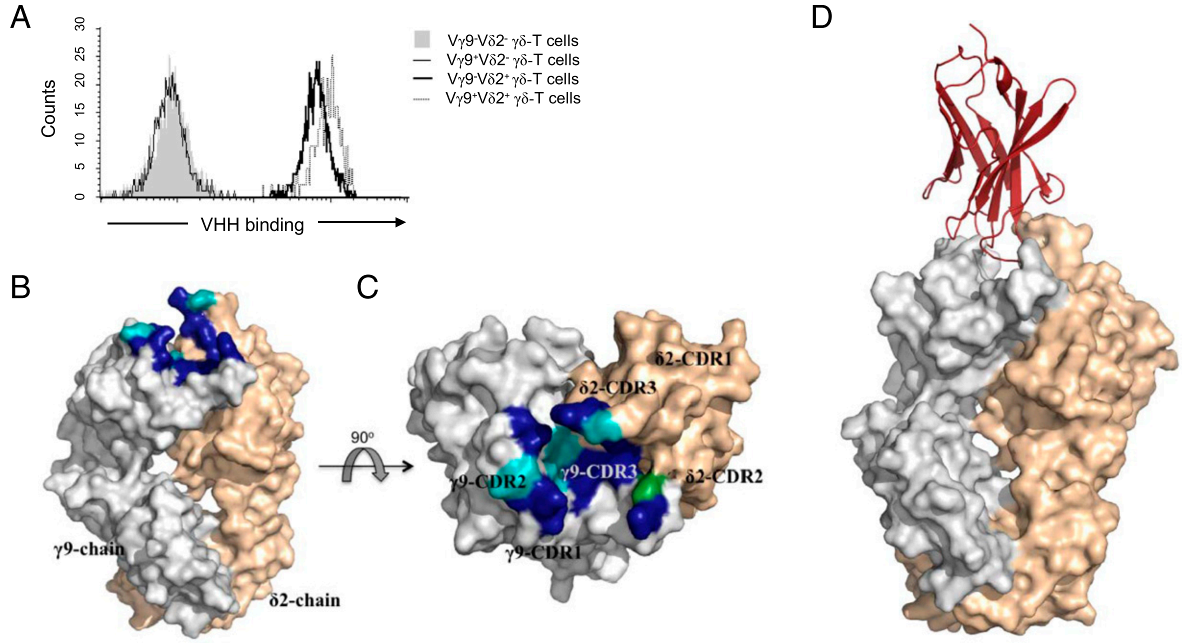

FIGURE 5. Vγ9Vδ2 TCR chain interactions with VHH 5E7 and BTN3A1. (**A**) Binding of VHH 5E7 to $V\gamma9^-V\delta2^-$ (filled gray), $V\gamma9^+V\delta2^-$ (thin line), $V\gamma9^-V\delta2^+$ (bold line), and $V\gamma9^+V\delta2^+$ (dotted line) γδ T cell populations as determined using flow cytometry. Results are representative of $n = 3$ experiments (biological replicates). (**B**) Surface representation of the Vγ9Vδ2 TCR (PDB code 1HXM). Residues of the δ2 chain and the γ9 chain are colored in silver and beige, respectively. The Vγ9Vδ2 TCR residues in the docking simulations that are found at the interface in both the interactions with VHH 5E7 and BTN3A1 (dark blue), only with VHH 5E7 (green), and only with BTN3A1 (light blue) are indicated. (**C**) A rotation and zoom on the binding region is reported with the same color scale as in (B). Labels on each Vγ9Vδ2 TCR CDR have been added. (**D**) Three-dimensional representation of the best HADDOCK cluster for the Vγ9Vδ2 TCR–VHH 5E7 complex (red).

whether binding of VHH 5E7 to the Vγ9Vδ2 TCR could directly compete for binding of BTN3A1 to the Vγ9Vδ2 TCR and thereby possibly account for the inhibitory effect of VHH 5E7, we additionally generated in silico models of the Vγ9Vδ2 TCR with BTN3A1 (the experimental structure of BTN3A1 is available as PDB code 4F9L) (7). Also in this case, in silico statistical contact analysis did not reveal any clear binding region on the Vγ9Vδ2 TCR, whereas a specific region could be identified on BTN3A1. The corresponding residues of BTN3A1, together with the solvent-exposed residues of the Vγ9Vδ2 TCR, were defined as active and passive residues, respectively, to drive a second docking (see Supplemental Table I). The results of this second run showed a clear preference for the Vγ9Vδ2 TCR to bind BTN3A1 with its CDRs, and in particular with residues in δ2 CDR3 (Gly^{101}, Glu^{102}, and Tyr^{103}), δ2 CDR1 (Ala^{32}, Ser^{34}, and Tyr^{36}), γ9 CDR2 (Tyr^{54}, Asp^{55}, and Arg^{59}), and γ9 CDR3 (Trp^{100}, Leu^{106}, and Lys^{109}). From the comparison of the docking results between the two complexes as illustrated in Fig. 5B and 5C (and Table I), we observed substantial overlap between the Vγ9Vδ2 TCR binding sites for VHH 5E7 and BTN3A1.

To further specify the Vγ9Vδ2 TCR binding sites interacting with VHH 5E7 and BTN3A1, we performed a third docking round with the most contacted residues from the second docking runs defined as active residues on both molecules to obtain a representative model for both complexes (details in *Materials and Methods* and list of residues reported in Supplemental Table I). For each complex, the top ranking HADDOCK cluster was selected for an analysis of the intermolecular interactions. In Table II a list of hydrogen bonds occurring at the interface is reported. As expected from the results of the previous runs, a clear overlap between the Vγ9Vδ2 TCR binding site for VHH 5E7 and BTN3A1 was noted, with particular involvement of the δ2 chain, especially in the binding with VHH 5E7 (see Table II). Fig. 5D shows a three-dimensional representation of the best HADDOCK cluster between the Vγ9Vδ2 TCR and VHH 5E7.

Taken together, these data indicate that VHH 5E7 and BTN3A1 could bind to overlapping regions on the Vγ9Vδ2 TCR, and they thereby suggest that the inhibitory effect of VHH 5E7 might be the result of active competition between VHH 5E7 and BTN3A1 for binding to the Vγ9Vδ2 TCR.

Table I. List of residues of the Vγ9Vδ2 TCR involved in the interaction with VHH 5E7 and BTN3A1

	TCR in Complex with VHH 5E7	TCR in Complex with BTN3A1
δ2 CDR3	**102**, **103**	101, **102**, **103**
γ9 CDR1	**32**	**32**, 34, 36
γ9 CDR2	**54**, **59**	**54**, 55, **59**
γ9 CDR3	**100**, **106**, 107, **109**	**100**, **106**, **109**

The Vγ9Vδ2 TCR residues involved both in the interactions with VHH 5E7 and with BTN3A1 are noted in bold type. Numbers indicate amino acid residues.

Vγ9Vδ2 TCR–specific VHH 5E7 inhibits NBP-mediated Vγ9Vδ2 T cell activation in PBMCs

Patients treated with NBP frequently experience a troublesome APR as a result of the (unintended) systemic activation of Vγ9Vδ2 T cells. NBP is frequently administered by i.v. infusion, resulting in the exposure of PBMCs to NBP for at least a few hours. Endocytically active cell types, including monocytes, are able to take up NBPs, leading to phosphoantigen accumulation and Vγ9Vδ2 T cell activation (56). We evaluated the capacity of the Vγ9Vδ2 TCR–specific VHH 5E7 to block this phenomenon. At present there is no satisfactory immunocompetent animal model available to study the inhibitory effects of VHH 5E7 in vivo, as rodents naturally lack BTN3A1 expression (57). In an effort to mimic the in vivo physiological situation ex vivo, we evaluated whether VHH 5E7 was capable of inhibiting Vγ9Vδ2 T cell

Table II. List of hydrogen bonds for Vγ9Vδ2 TCR–BTN3A1 and Vγ9Vδ2 TCR–VHH 5E7 complexes

Vγ9Vδ2 TCR		BTN3A1		Vγ9Vδ2 TCR		VHH 5E7	
δ2, 102	Glu	27	Arg	δ2, 34	Tyr	3	Gln
δ2, 102	Glu	1	Glu	δ2, 97	Leu	3	Gln
δ2, 102	Glu	119	Tyr	δ2, 100	Gly	109	Lys
δ2, 103	Tyr	103	Ala	δ2, 99	Met	5	Ser
γ9, 55	Asp	30	Ser	δ2, 103	Tyr	28	Phe
γ9, 54	Tyr	31	Asn	γ9, 54	Tyr	80	Gly
δ2, 101	Gly	99	Gln	γ9, 59	Arg	26	His
γ9, 59	Arg	30	Ser				
γ9, 107	Gly	104	Asp				

Based on the top clusters obtained by docking. Numbers indicate amino acid residues.

activation in PBMCs of healthy adult volunteers exposed to NBP. PBMCs were preincubated with VHH 5E7 followed by a 2 h culture in the presence of NBP. After washing, the PBMCs were cultured for an additional 24 h, after which Vγ9Vδ2 T cell activation was determined by assessing upregulation of CD25 and CD69 by flow cytometry. VHH 5E7 was able to significantly inhibit the NBP-induced activation of peripheral blood Vγ9Vδ2 T cells at concentrations as low as 100 nM VHH (Fig. 6).

Inhibition of tumor cell–mediated activation of Vγ9Vδ2 T cells

As VHH 5E7 efficiently inhibited Vγ9Vδ2 T cell activation after NBP stimulation, we next explored whether it could also block Vγ9Vδ2 T cell activation induced by tumor cells known to promote elevated levels of phosphoantigen without the requirement of exogenous agents. The Burkitt's lymphoma cell line Daudi induces continuous activation of Vγ9Vδ2 T cells, as do some malignancies such as, for example, chronic lymphocytic leukemia (CLL) (58, 59). Vγ9Vδ2 T cells were incubated with either VHH 5E7 or a nonspecific control VHH and cocultured with Daudi cells in a 1:1 ratio. Mevastatin, which diminishes intracellular phosphoantigen levels by inhibiting hydroxymethylglutaryl CoA reductase, an enzyme early in the mevalonate pathway, was used to determine the background level of Vγ9Vδ2 T cell activation whereas NBP was used to determine the maximum level of Vγ9Vδ2 T cell activation in this experimental system (17, 60). Degranulation of Vγ9Vδ2 T cells and Vγ9Vδ2 T cell–induced Daudi cell lysis was assessed after 4 h by flow cytometry. VHH 5E7 significantly blocked the activation of Vγ9Vδ2 T cells triggered by Daudi cells in a concentration-dependent manner, as assessed by both degranulation and target cell lysis (Fig. 7). Indeed, both the Vγ9Vδ2 T cell CD107a levels as well as Daudi cell lysis in the presence of VHH 5E7 were as low as observed when Vγ9Vδ2 T cells were cocultured with mevastatin-treated Daudi cells. Furthermore, VHH 5E7 was also capable of neutralizing the increased activation of Vγ9Vδ2 T cells resulting from NBP treatment of Daudi cells. The Vγ9Vδ2 T cell CD3 expression level was not altered during these coculture experiments (Supplemental Fig. 2), indicating that VHH 5E7 does not act by downregulating the Vγ9Vδ2 TCR but by blocking the Vγ9Vδ2 TCR from recognizing the phosphoantigen–BTN3A1 complex. Taken together, these data indicate that VHH 5E7 can efficiently neutralize tumor cell–induced Vγ9Vδ2 T cell activation.

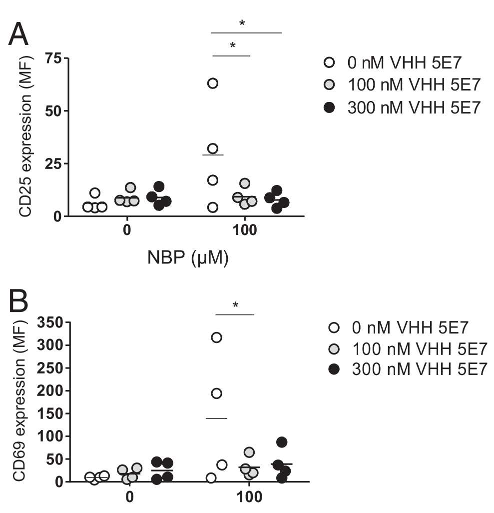

FIGURE 6. VHH 5E7 inhibits Vγ9Vδ2 T cell activation in NBP-exposed PBMCs. PBMCs from a healthy adult donor were preincubated without VHH (white), with 100 nM VHH (gray), or with 300 nM VHH (black), treated with NBP for 2 h, washed, and then cultured for an additional 24 h. Vγ9Vδ2 T cell activation was assessed by determining CD25 (**A**) and CD69 (**B**) upregulation on Vγ9Vδ2 T cells within the PBMC pool. Shown are means ± SEM of $n = 4$ experiments (biological replicates). The p values were calculated with a two-way ANOVA and a Bonferroni post hoc test. *$p < 0.05$. MF, mean fluorescence intensity.

Discussion

In this study, we report on the identification and characterization of a Vγ9Vδ2 TCR–specific VHH that binds with high affinity and has neutralizing properties. Although Vγ9Vδ2 T cells play an important role in antitumor and antimicrobial defense, there are circumstances in which Vγ9Vδ2 T cell activation can be considered detrimental to the host. For instance, when NBPs are given to patients for the treatment of hypercalcemia, osteoporosis, or metastatic bone disease, bothersome side effects resembling an APR are frequently observed (15–17). It is thought that the unintended accumulation of the phosphoantigen isopentenyl pyrophosphate (IPP) induced by NBPs stimulates a massive Vγ9Vδ2 T cell activation with accompanying high levels of proinflammatory cytokine production that leads to the APR. Recently, clinical attempts have been made to reduce the APR effects observed with NBP treatment by coadministering statin medication, which inhibits an upstream step in the mevalonate pathway, thereby preventing IPP accumulation, at least in vitro (17, 18, 59–61). However, statin therapy could not prevent activation of Vγ9Vδ2 T cells or the occurrence of an APR in vivo, which is likely related to insufficient inhibition of the mevalonate pathway at doses commonly used for its therapeutic indication as a cholesterol lowering agent (23–25). VHH 5E7 might provide a novel therapeutic approach, as it directly targets the Vγ9Vδ2 TCR and blocks the phosphoantigen/BTN3A1-mediated Vγ9Vδ2 T cell activation in patients treated with NBPs. Indeed, VHH 5E7 significantly inhibited the activation and cytokine production of human Vγ9Vδ2 T cell lines derived from various donors, when stimulated by human NBP-exposed cells. Although Vδ2 TCR–specific mAbs

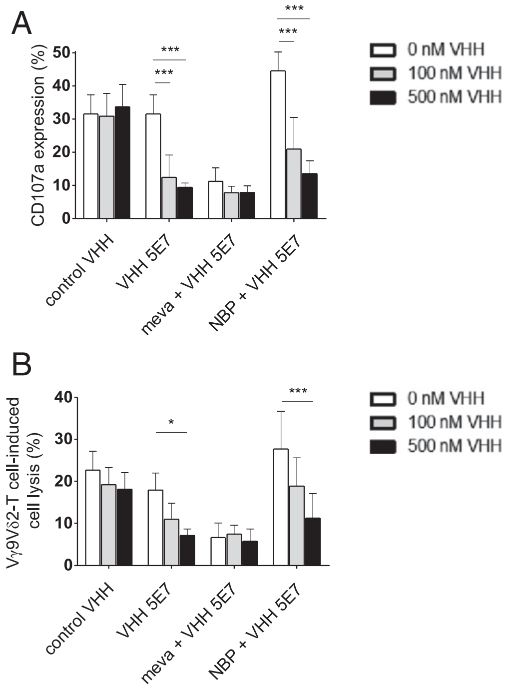

FIGURE 7. VHH 5E7 inhibits tumor cell–induced Vγ9Vδ2 T cell activation. Vγ9Vδ2 T cells were incubated with VHH 5E7 or a nonspecific control VHH (white, 0 nM VHH; gray, 100 nM VHH; black, 500 nM VHH) and cocultured with mevastatin-treated, NBP-treated, or regular Daudi cells in a 1:1 ratio. After 4 h, Vγ9Vδ2 T cell activation was determined by assessing CD107a expression on Vγ9Vδ2 T cells (**A**) and assessing Vγ9Vδ2 T cell–induced lysis of Daudi cells (**B**). The percentage of lysed Daudi cells was determined using 7-AAD staining and flow cytometry. Shown are means ± SEM of $n = 3$ experiments (biological replicates). The p values were calculated with a two-way ANOVA and a Bonferroni post hoc test. $*p < 0.05$, $***p < 0.001$. meva, mevastatin.

with neutralizing properties have been described, the clinical use of these mAbs would have several limitations, including the development of human anti-mouse Abs, resulting in Ab neutralization and potential adverse events such as the cytokine release syndrome (27, 62). When considering clinical application, VHHs have several advantages over conventional mAbs. For example, VHHs are low immunogenic because they are devoid of an Fc region and share high homology with human VH family three genes. Furthermore, owing to the single-domain character and small size (~15 kDa) of VHHs, they have additional advantages, including enhanced tissue/tumor penetration, enhanced stability and solubility, and ease of production in relatively cost- and time-efficient production systems such as bacteria or yeast (27, 63).

Because rodents naturally lack BTN3A1 expression and hence phosphoantigen-dependent γδ T cell responses, there is currently no satisfactory immunocompetent rodent model available to investigate the inhibitory effects of VHH 5E7 on Vγ9Vδ2 T cell activation in vivo (57). Therefore, we studied the effect of VHH 5E7 on preventing NBP-induced Vγ9Vδ2 T cell activation directly ex vivo using PBMCs of healthy adult volunteers, confirming its neutralizing properties. Furthermore, as VHH 5E7 has high affinity for the Vγ9Vδ2 TCR and could still be detected on the cell surface of Vγ9Vδ2 T cells after >14 d in culture, our data offer a promising perspective to explore this VHH as a novel therapeutic to prevent the occurrence of APR in patients treated with NBPs.

Additionally, we found that VHH 5E7 can inhibit Vγ9Vδ2 T cell activation when exposed to tumor cells that induce continuous Vγ9Vδ2 T cell activation without the requirement of additional agents to promote elevated levels of phosphoantigen. Multiple studies have reported on the induction of Vγ9Vδ2 T cell unresponsiveness after repeated administration of NBP or exogenous phosphoantigens (64–66). Likewise, it has been reported that patients with, for example relapsed/refractory low-grade non–Hodgkin lymphoma, multiple myeloma, or CLL can have an unresponsive Vγ9Vδ2 T cell population (11, 58). Although it is unknown what causes the Vγ9Vδ2 T cell unresponsiveness in these patients, it has been suggested that an overactive mevalonate pathway, resulting in supraphysiologic levels of the phosphoantigen IPP, leads to continuous Vγ9Vδ2 T cell activation and exhaustion in patients with CLL (58, 67). An unresponsive Vγ9Vδ2 T cell population can severely limit the efficacy of Vγ9Vδ2 T cell–dependent antitumor immune responses. It would be worth investigating whether VHH 5E7 could inhibit this continuous Vγ9Vδ2 T cell activation mediated by tumor cells and could thereby restore Vγ9Vδ2 T cell anergy and exhaustion and allow Vγ9Vδ2 T cells to regain their antitumor effector function. If so, administration of VHH 5E7 might not only also be beneficial for non–Hodgkin lymphoma and multiple myeloma patients but, as Vγ9Vδ2 T cells recognize a broad range of cancer cells, it is not unlikely that Vγ9Vδ2 T cell exhaustion and reduced antitumor function also occur in nonhematological cancers (2, 10, 68, 69). To date, there are limited reports about the mechanism behind the observed dysfunctional Vγ9Vδ2 T cell population in patients; consequently, it would be interesting to investigate the mevalonate pathway activity in patients from a broad range of cancer types and correlate this to patients' Vγ9Vδ2 T cell responsiveness. If a strong correlation is found, VHH 5E7 may be clinically relevant to prevent the diminished Vγ9Vδ2 T cell–mediated antitumor immune response in these patients.

Of note, we found that VHH 5E7 not only neutralized phosphoantigen-dependent, but also phosphoantigen-independent, Vγ9Vδ2 T cell activation by the activating anti-BTN3A1 mAb 20.1. In vitro and in silico binding analyses revealed VHH 5E7 to predominantly bind to the Vδ2 chain of the Vγ9Vδ2 TCR. VHH 5E7 did not induce downregulation of the Vγ9Vδ2 TCR, and it is therefore likely that VHH 5E7 exerts its inhibitory function by shielding the Vγ9Vδ2 TCR from interacting with BTN3A1-expressing cells. Currently, there is an ongoing debate in the literature on the exact mode of recognition between Vγ9Vδ2 T cells and BTN3A1-expressing cells. Although the requirement of intracellular binding of phosphoantigen to BTN3A1 has been demonstrated by several groups (8, 54, 57, 70), diverse models have been proposed to explain the extracellular interactions between Vγ9Vδ2 T cells and BTN3A1-expressing cells (55, 71, 72). Of interest, docking simulations that we performed suggested a direct interaction between BTN3A1 and the Vγ9Vδ2 TCR and additionally suggested that the predicted region of interaction overlapped with the region on the Vγ9Vδ2 TCR predicted to interact with VHH 5E7. However, although this could explain the observed inhibitory effects of VHH 5E7, it does not explain or take into account reports indicating additional proteins encoded on chromosome 6 supplementary to BTN3A1 to be required for full HMPBB-induced stimulation of Vγ9Vδ2 T cells (55, 73). Possibly, our observed in silico interaction between BTN3A1 and the Vγ9Vδ2 TCR is of relatively low affinity, which would be in agreement with earlier reports (55) and suggestions (8) and would therefore require additional (costimulatory) interactions for complete TCR engagement and Vγ9Vδ2 T cell activation (74).

Previously, mutagenesis experiments have shown that variations in the Vγ9Vδ2 TCR CDR3δ2 region, which may differ within and between individuals, determine phosphoantigen/BTN3A1-mediated Vγ9Vδ2 TCR activation. However, no specific sequence was required except for an aliphatic residue at position 97 and restrictions regarding the length of the CDR (10, 75). In accordance with these data, one of the interactions found in the model of the Vγ9Vδ2 TCR–VHH 5E7 complex involves CDR3δ2 Leu^{97}, and although interactions were found in the $CDR3\delta2_{98-103}$ region, reported to affect phosphoantigen/BTN3A1-mediated Vγ9Vδ2 T cell activation (10), mutations in this region did not abrogate VHH 5E7 binding (Supplemental Fig. 3), suggesting that VHH 5E7 will be widely applicable when considering clinical utility. It is likely that the CDR3δ2 Leu^{97} residue plays a crucial role in the strong neutralizing effect of VHH 5E7 on Vγ9Vδ2 TCR activation. Additionally, interactions were also predicted for the Vγ9 chain with VHH 5E7 and BTN3A1. Both molecules were found to interact with γ9 Lys^{109}, a residue previously reported to be involved in Vγ9Vδ2 TCR activation (76, 77). Considering the relevance of the δ2 chain interactions reported in the present study and previously (10, 78), the γ9 interactions are likely to be primarily relevant for stabilization of the interaction with Vδ2. Additionally, we found residue γ9 Tyr^{54} to interact with BTN3A1 but not with VHH 5E7, which is in accordance with the suggestion that this residue is involved in contacting the Ag-presenting molecule of the Vγ9Vδ2 TCR (75).

Collectively, the data reported in the present study show that we have identified a unique Vγ9Vδ2 T cell–specific VHH that can inhibit Vγ9Vδ2 T cell activation by directly targeting the Vγ9Vδ2 TCR. This VHH holds promise for the development of a future immunotherapeutic strategy aimed at preventing undesired Vγ9Vδ2 T cell activation as, for example, observed during the APR in NBP-treated patients.

Disclosures

R.C.G.d.B., H.J.v.d.V., T.D.d.G., and H.M.W.V. have a patent on Vγ9Vδ2 T cell–specific VHHs. J.K. is the inventor of multiple patents dealing with γδTCRs and is a cofounder as well as chief scientific officer of Gadeta. The other authors have no financial conflicts of interest.

References

1. Fowler, D. W., and M. D. Bodman-Smith. 2015. Harnessing the power of Vδ2 cells in cancer immunotherapy. *Clin. Exp. Immunol.* 180: 1–10.
2. Bouet-Toussaint, F., F. Cabillic, O. Toutirais, M. Le Gallo, C. Thomas de la Pintière, P. Daniel, N. Genetet, B. Meunier, E. Dupont-Bierre, K. Boudjema, and V. Catros. 2008. Vγ9Vδ2 T cell-mediated recognition of human solid tumors. Potential for immunotherapy of hepatocellular and colorectal carcinomas. *Cancer Immunol. Immunother.* 57: 531–539.
3. Constant, P., F. Davodeau, M. A. Peyrat, Y. Poquet, G. Puzo, M. Bonneville, and J. J. Fournié. 1994. Stimulation of human gamma delta T cells by nonpeptidic mycobacterial ligands. *Science* 264: 267–270.
4. Tanaka, Y., C. T. Morita, Y. Tanaka, E. Nieves, M. B. Brenner, and B. R. Bloom. 1995. Natural and synthetic non-peptide antigens recognized by human γδ T cells. *Nature* 375: 155–158.
5. Fournié, J. J., and M. Bonneville. 1996. Stimulation of γδ T cells by phosphoantigens. *Res. Immunol.* 147: 338–347.
6. Caccamo, N., F. Dieli, S. Meraviglia, G. Guggino, and A. Salerno. 2010. γδ T cell modulation in anticancer treatment. *Curr. Cancer Drug Targets* 10: 27–36.
7. Palakodeti, A., A. Sandstrom, L. Sundaresan, C. Harly, S. Nedellec, D. Olive, E. Scotet, M. Bonneville, and E. J. Adams. 2012. The molecular basis for modulation of human Vγ9Vδ2 T cell responses by CD277/butyrophilin-3 (BTN3A)-specific antibodies. *J. Biol. Chem.* 287: 32780–32790.
8. Sandstrom, A., C.-M. Peigné, A. Léger, J. E. Crooks, F. Konczak, M.-C. Gesnel, R. Breathnach, M. Bonneville, E. Scotet, and E. J. Adams. 2014. The intracellular B30.2 domain of butyrophilin 3A1 binds phosphoantigens to mediate activation of human Vγ9Vδ2 T cells. *Immunity* 40: 490–500.
9. Sebestyen, Z., W. Scheper, A. Vyborova, S. Gu, Z. Rychnavska, M. Schiffler, A. Cleven, C. Chéneau, M. van Noorden, C.-M. Peigné, et al. 2016. RhoB mediates phosphoantigen recognition by Vγ9Vδ2 T cell receptor. *Cell Reports* 15: 1973–1985.
10. Gründer, C., S. van Dorp, S. Hol, E. Drent, T. Straetemans, S. Heijhuurs, K. Scholten, W. Scheper, Z. Sebestyen, A. Martens, et al. 2012. γ9 and δ2CDR3 domains regulate functional avidity of T cells harboring γ9δ2TCRs. *Blood* 120: 5153–5162.
11. Wilhelm, M., V. Kunzmann, S. Eckstein, P. Reimer, F. Weissinger, T. Ruediger, and H.-P. Tony. 2003. γδ T cells for immune therapy of patients with lymphoid malignancies. *Blood* 102: 200–206.
12. Dieli, F., D. Vermijlen, F. Fulfaro, N. Caccamo, S. Meraviglia, G. Cicero, A. Roberts, S. Buccheri, M. D'Asaro, N. Gebbia, et al. 2007. Targeting human γδ T cells with zoledronate and interleukin-2 for immunotherapy of hormone-refractory prostate cancer. *Cancer Res.* 67: 7450–7457.
13. Eberl, M., G. W. Roberts, S. Meuter, J. D. Williams, N. Topley, and B. Moser. 2009. A rapid crosstalk of human γδ T cells and monocytes drives the acute inflammation in bacterial infections. *PLoS Pathog.* 5: e1000308.
14. Wang, L., A. Kamath, H. Das, L. Li, and J. F. Bukowski. 2001. Antibacterial effect of human Vγ2Vδ2 T cells in vivo. *J. Clin. Invest.* 108: 1349–1357.
15. Nussbaum, S. R., J. Younger, C. J. Vandepol, R. F. Gagel, M. A. Zubler, R. Chapman, I. C. Henderson, and L. E. Mallette. 1993. Single-dose intravenous therapy with pamidronate for the treatment of hypercalcemia of malignancy: comparison of 30-, 60-, and 90-mg dosages. *Am. J. Med.* 95: 297–304.
16. Adami, S., A. K. Bhalla, R. Dorizzi, F. Montesanti, S. Rosini, G. Salvagno, and V. Lo Cascio. 1987. The acute-phase response after bisphosphonate administration. *Calcif. Tissue Int.* 41: 326–331.
17. Hewitt, R. E., A. Lissina, A. E. Green, E. S. Slay, D. A. Price, and A. K. Sewell. 2005. The bisphosphonate acute phase response: rapid and copious production of proinflammatory cytokines by peripheral blood gd T cells in response to aminobisphosphonates is inhibited by statins. *Clin. Exp. Immunol.* 139: 101–111.
18. Sauty, A., M. Pecherstorfer, I. Zimmer-Roth, P. Fioroni, L. Juillerat, M. Markert, H. Ludwig, P. Leuenberger, P. Burckhardt, and D. Thiebaud. 1996. Interleukin-6 and tumor necrosis factor α levels after bisphosphonates treatment in vitro and in patients with malignancy. *Bone* 18: 133–139.
19. Kunzmann, V., E. Bauer, and M. Wilhelm. 1999. γ/δ T-cell stimulation by pamidronate. *N. Engl. J. Med.* 340: 737–738.
20. Fisher, J. E., M. J. Rogers, J. M. Halasy, S. P. Luckman, D. E. Hughes, P. J. Masarachia, G. Wesolowski, R. G. Russell, G. A. Rodan, and A. A. Reszka. 1999. Alendronate mechanism of action: geranylgeraniol, an intermediate in the mevalonate pathway, prevents inhibition of osteoclast formation, bone resorption, and kinase activation in vitro. *Proc. Natl. Acad. Sci. USA* 96: 133–138.
21. Coxon, F. P., and M. J. Rogers. 2003. The role of prenylated small GTP-binding proteins in the regulation of osteoclast function. *Calcif. Tissue Int.* 72: 80–84.
22. Kobayashi, H., and Y. Tanaka. 2015. γδ T cell immunotherapy—a review. *Pharmaceuticals (Basel)* 8: 40–61.
23. Srivastava, T., C. J. Haney, and U. S. Alon. 2009. Atorvastatin may have no effect on acute phase reaction in children after intravenous bisphosphonate infusion. *J. Bone Miner. Res.* 24: 334–337.
24. Makras, P., A. D. Anastasilakis, S. A. Polyzos, I. Bisbinas, G. T. Sakellariou, and S. E. Papapoulos. 2011. No effect of rosuvastatin in the zoledronate-induced acute-phase response. *Calcif. Tissue Int.* 88: 402–408.
25. Thompson, K., F. Keech, D. J. McLernon, K. Vinod, R. J. May, W. G. Simpson, M. J. Rogers, and D. M. Reid. 2011. Fluvastatin does not prevent the acute-phase response to intravenous zoledronic acid in post-menopausal women. *Bone* 49: 140–145.
26. van der Linden, R. H., L. G. Frenken, B. de Geus, M. M. Harmsen, R. C. Ruuls, W. Stok, L. de Ron, S. Wilson, P. Davis, and C. T. Verrips. 1999. Comparison of physical chemical properties of llama VHH antibody fragments and mouse monoclonal antibodies. *Biochim. Biophys. Acta* 1431: 37–46.
27. Harmsen, M. M., and H. J. De Haard. 2007. Properties, production, and applications of camelid single-domain antibody fragments. *Appl. Microbiol. Biotechnol.* 77: 13–22.
28. de Marco, A. 2011. Biotechnological applications of recombinant single-domain antibody fragments. *Microb. Cell Fact.* 10: 44.
29. Roovers, R. C., T. Laeremans, L. Huang, S. De Taeye, A. J. Verkleij, H. Revets, H. J. de Haard, and P. M. van Bergen en Henegouwen. 2007. Efficient inhibition of EGFR signaling and of tumour growth by antagonistic anti-EFGR nanobodies. *Cancer Immunol. Immunother.* 56: 303–317.
30. de Bruin, R. C. G., S. M. Lougheed, L. van der Kruk, A. G. Stam, E. Hooijberg, R. C. Roovers, P. M. P. van Bergen En Henegouwen, H. M. W. Verheul, T. D. de Gruijl, and H. J. van der Vliet. 2016. Highly specific and potently activating Vγ9Vδ2-T cell specific nanobodies for diagnostic and therapeutic applications. *Clin. Immunol.* 169: 128–138.
31. Schneiders, F. L., R. C. G. de Bruin, S. J. A. M. Santegoets, M. Bonneville, E. Scotet, R. J. Scheper, H. M. W. Verheul, T. D. de Gruijl, and H. J. van der Vliet. 2012. Activated iNKT cells promote Vγ9Vδ2-T cell anti-tumor effector functions through the production of TNF-α. *Clin. Immunol.* 142: 194–200.
32. Yssel, H., J. E. De Vries, M. Koken, W. Van Blitterswijk, and H. Spits. 1984. Serum-free medium for generation and propagation of functional human cytotoxic and helper T cell clones. *J. Immunol. Methods* 72: 219–227.
33. Scholten, K. B. J., D. Kramer, E. W. M. Kueter, M. Graf, T. Schoedl, C. J. L. M. Meijer, M. W. J. Schreurs, and E. Hooijberg. 2006. Codon modification of T cell receptors allows enhanced functional expression in transgenic human T cells. *Clin. Immunol.* 119: 135–145.
34. Allison, T. J., C. C. Winter, J. J. Fournié, M. Bonneville, and D. N. Garboczi. 2001. Structure of a human γδ T-cell antigen receptor. *Nature* 411: 820–824.
35. Davodeau, F., M. A. Peyrat, M. M. Hallet, I. Houde, H. Vie, and M. Bonneville. 1993. Peripheral selection of antigen receptor junctional features in a major human gamma delta subset. *Eur. J. Immunol.* 23: 804–808.
36. Kjer-Nielsen, L., N. A. Borg, D. G. Pellicci, T. Beddoe, L. Kostenko, C. S. Clements, N. A. Williamson, M. J. Smyth, G. S. Besra, H. H. Reid, et al. 2006. A structural basis for selection and cross-species reactivity of the semi-invariant NKT cell receptor in CD1d/glycolipid recognition. *J. Exp. Med.* 203: 661–673.
37. Hoogenboom, H. R., A. D. Griffiths, K. S. Johnson, D. J. Chiswell, P. Hudson, and G. Winter. 1991. Multi-subunit proteins on the surface of filamentous phage: methodologies for displaying antibody (Fab) heavy and light chains. *Nucleic Acids Res.* 19: 4133–4137.

38. Altschul, S. F., W. Gish, W. Miller, E. W. Myers, and D. J. Lipman. 1990. Basic local alignment search tool. *J. Mol. Biol.* 215: 403–410.
39. Berman, H. M., J. Westbrook, Z. Feng, G. Gilliland, T. N. Bhat, H. Weissig, I. N. Shindyalov, and P. E. Bourne. 2000. The Protein Data Bank. *Nucleic Acids Res.* 28: 235–242.
40. Schmitz, K. R., A. Bagchi, R. C. Roovers, P. M. van Bergen en Henegouwen, and K. M. Ferguson. 2013. Structural evaluation of EGFR inhibition mechanisms for nanobodies/VHH domains. *Structure* 21: 1214–1224.
41. Sali, A., and T. L. Blundell. 1993. Comparative protein modelling by satisfaction of spatial restraints. *J. Mol. Biol.* 234: 779–815.
42. Shen, M.-Y., and A. Sali. 2006. Statistical potential for assessment and prediction of protein structures. *Protein Sci.* 15: 2507–2524.
43. Dominguez, C., R. Boelens, and A. M. J. J. Bonvin. 2003. HADDOCK: a protein–protein docking approach based on biochemical or biophysical information. *J. Am. Chem. Soc.* 125: 1731–1737.
44. de Vries, S. J., A. D. J. van Dijk, M. Krzeminski, M. van Dijk, A. Thureau, V. Hsu, T. Wassenaar, and A. M. J. J. Bonvin. 2007. HADDOCK versus HADDOCK: new features and performance of HADDOCK2.0 on the CAPRI targets. *Proteins* 69: 726–733.
45. van Zundert, G. C. P., J. P. G. L. M. Rodrigues, M. Trellet, C. Schmitz, P. L. Kastritis, E. Karaca, A. S. J. Melquiond, M. van Dijk, S. J. de Vries, and A. M. J. J. Bonvin. 2015. The HADDOCK2.2 Web server: user-friendly integrative modeling of biomolecular complexes. *J. Mol. Biol.* 428: 720–725.
46. Brünger, A. T., P. D. Adams, G. M. Clore, W. L. DeLano, P. Gros, R. W. Grosse-Kunstleve, J. S. Jiang, J. Kuszewski, M. Nilges, N. S. Pannu, et al. 1998. Crystallography & NMR system: a new software suite for macromolecular structure determination. *Acta Crystallogr. D Biol. Crystallogr.* 54: 905–921.
47. Fernández-Recio, J., M. Totrov, and R. Abagyan. 2004. Identification of protein–protein interaction sites from docking energy landscapes. *J. Mol. Biol.* 335: 843–865.
48. Vangone, A., R. Oliva, and L. Cavallo. 2012. CONS-COCOMAPS: a novel tool to measure and visualize the conservation of inter-residue contacts in multiple docking solutions. *BMC Bioinformatics* 13(Suppl. 4): S19.
49. Nedellec, S., M. Bonneville, and E. Scotet. 2010. Human Vγ9Vδ2 T cells: from signals to functions. *Semin. Immunol.* 22: 199–206.
50. Osborne, D. G., and S. A. Wetzel. 2012. Trogocytosis results in sustained intracellular signaling in $CD4^+$ T cells. *J. Immunol.* 189: 4728–4739.
51. Poupot, M., F. Pont, and J.-J. Fournié. 2005. Profiling blood lymphocyte interactions with cancer cells uncovers the innate reactivity of human γδ T cells to anaplastic large cell lymphoma. *J. Immunol.* 174: 1717–1722.
52. Schneiders, F. L., J. Prodöhl, J. M. Ruben, T. O'Toole, R. J. Scheper, M. Bonneville, E. Scotet, H. M. W. Verheul, T. D. de Gruijl, and H. J. van der Vliet. 2014. CD1d-restricted antigen presentation by Vγ9Vδ2-T cells requires trogocytosis. *Cancer Immunol. Res.* 2: 732–740.
53. Rossi, E. A., D. L. Rossi, T. M. Cardillo, C.-H. Chang, and D. M. Goldenberg. 2014. Redirected T-cell killing of solid cancers targeted with an anti-CD3/Trop-2-bispecific antibody is enhanced in combination with interferon-α. *Mol. Cancer Ther.* 13: 2341–2351.
54. Harly, C., Y. Guillaume, S. Nedellec, C.-M. Peigné, H. Mönkkönen, J. Mönkkönen, J. Li, J. Kuball, E. J. Adams, S. Netzer, et al. 2012. Key implication of CD277/butyrophilin-3 (BTN3A) in cellular stress sensing by a major human γδ T-cell subset. *Blood* 120: 2269–2279.
55. Vavassori, S., A. Kumar, G. S. Wan, G. S. Ramanjaneyulu, M. Cavallari, S. El Daker, T. Beddoe, A. Theodossis, N. K. Williams, E. Gostick, et al. 2013. Butyrophilin 3A1 binds phosphorylated antigens and stimulates human γδ T cells. *Nat. Immunol.* 14: 908–916.
56. Welton, J. L., M. P. Morgan, S. Martí, M. D. Stone, B. Moser, A. K. Sewell, J. Turton, and M. Eberl. 2013. Monocytes and γδ T cells control the acute-phase response to intravenous zoledronate: insights from a phase IV safety trial. *J. Bone Miner. Res.* 28: 464–471.
57. Wang, H., O. Henry, M. D. Distefano, Y.-C. Wang, J. Räikkönen, J. Mönkkönen, Y. Tanaka, and C. T. Morita. 2013. Butyrophilin 3A1 plays an essential role in prenyl pyrophosphate stimulation of human Vγ2Vδ2 T cells. *J. Immunol.* 191: 1029–1042.
58. Coscia, M., C. Vitale, S. Peola, M. Foglietta, M. Rigoni, V. Griggio, B. Castella, D. Angelini, S. Chiaretti, C. Riganti, et al. 2012. Dysfunctional Vγ9Vδ2 T cells are negative prognosticators and markers of dysregulated mevalonate pathway activity in chronic lymphocytic leukemia cells. *Blood* 120: 3271–3279.
59. Gober, H.-J., M. Kistowska, L. Angman, P. Jenö, L. Mori, and G. De Libero. 2003. Human T cell receptor γδ cells recognize endogenous mevalonate metabolites in tumor cells. *J. Exp. Med.* 197: 163–168.
60. Thompson, K., and M. J. Rogers. 2004. Statins prevent bisphosphonate-induced γ,δ-T-cell proliferation and activation in vitro. *J. Bone Miner. Res.* 19: 278–288.
61. Gogoi, D., and S. V. Chiplunkar. 2013. Targeting gamma delta T cells for cancer immunotherapy: bench to bedside. *Indian J. Med. Res.* 138: 755–761.
62. Lameris, R., R. C. G. de Bruin, F. L. Schneiders, P. M. van Bergen en Henegouwen, H. M. Verheul, T. D. de Gruijl, and H. J. van der Vliet. 2014. Bispecific antibody platforms for cancer immunotherapy. *Crit. Rev. Oncol. Hematol.* 92: 153–165.
63. Tijink, B. M., T. Laeremans, M. Budde, M. Stigter-van Walsum, T. Dreier, H. J. de Haard, C. R. Leemans, and G. A. M. S. van Dongen. 2008. Improved tumor targeting of anti-epidermal growth factor receptor nanobodies through albumin binding: taking advantage of modular nanobody technology. *Mol. Cancer Ther.* 7: 2288–2297.
64. Sicard, H., S. Ingoure, B. Luciani, C. Serraz, J.-J. Fournié, M. Bonneville, J. Tiollier, and F. Romagné. 2005. In vivo immunomanipulation of Vγ9Vδ2 T cells with a synthetic phosphoantigen in a preclinical nonhuman primate model. *J. Immunol.* 175: 5471–5480.
65. Cendron, D., S. Ingoure, A. Martino, R. Casetti, F. Horand, F. Romagné, H. Sicard, J.-J. Fournié, and F. Poccia. 2007. A tuberculosis vaccine based on phosphoantigens and fusion proteins induces distinct γδ and αβ T cell responses in primates. *Eur. J. Immunol.* 37: 549–565.
66. Poupot, M., F. Boissard, D. Betous, L. Bardouillet, S. Fruchon, F. L'Faqihi-Olive, F. Pont, M. Mekaouche, S. Ingoure, H. Sicard, et al. 2014. The PPARα pathway in Vγ9Vδ2 T cell anergy. *Cell. Mol. Biol. Lett.* 19: 649–658.
67. Braza, M. S., and B. Klein. 2013. Anti-tumour immunotherapy with Vγ9Vδ2 T lymphocytes: from the bench to the bedside. *Br. J. Haematol.* 160: 123–132.
68. Viey, E., G. Fromont, B. Escudier, Y. Morel, S. Da Rocha, S. Chouaib, and A. Caignard. 2005. Phosphostim-activated γδ T cells kill autologous metastatic renal cell carcinoma. *J. Immunol.* 174: 1338–1347.
69. Sicard, H., T. Al Saati, G. Delsol, and J. J. Fournié. 2001. Synthetic phosphoantigens enhance human Vγ9Vδ2 T lymphocytes killing of non-Hodgkin's B lymphoma. *Mol. Med.* 7: 711–722.
70. Rhodes, D. A., H.-C. Chen, A. J. Price, A. H. Keeble, M. S. Davey, L. C. James, M. Eberl, and J. Trowsdale. 2015. Activation of human γδ T cells by cytosolic interactions of BTN3A1 with soluble phosphoantigens and the cytoskeletal adaptor periplakin. *J. Immunol.* 194: 2390–2398.
71. Wang, H., and C. T. Morita. 2015. Sensor function for butyrophilin 3A1 in prenyl pyrophosphate stimulation of human Vγ2Vδ2 T cells. *J. Immunol.* 195: 4583–4594.
72. De Libero, G., S.-Y. Lau, and L. Mori. 2015. Phosphoantigen presentation to TCR γδ cells, a conundrum getting less gray zones. *Front. Immunol.* 5: 679.
73. Riaño, F., M. M. Karunakaran, L. Starick, J. Li, C. J. Scholz, V. Kunzmann, D. Olive, S. Amslinger, and T. Herrmann. 2014. Vγ9Vδ2 TCR-activation by phosphorylated antigens requires butyrophilin 3 A1 (BTN3A1) and additional genes on human chromosome 6. *Eur. J. Immunol.* 44: 2571–2576.
74. Kilcollins, A. M., J. Li, C.-H. C. Hsiao, and A. J. Wiemer. 2016. HMBPP analog prodrugs bypass energy-dependent uptake to promote efficient BTN3A1-mediated malignant cell lysis by Vγ9Vδ2 T lymphocyte effectors. *J. Immunol.* 197: 419–428.
75. Wang, H., Z. Fang, and C. T. Morita. 2010. Vγ2Vδ2 T cell receptor recognition of prenyl pyrophosphates is dependent on all CDRs. *J. Immunol.* 184: 6209–6222.
76. Miyagawa, F., Y. Tanaka, S. Yamashita, B. Mikami, K. Danno, M. Uehara, and N. Minato. 2001. Essential contribution of germline-encoded lysine residues in Jγ1.2 segment to the recognition of nonpeptide antigens by human γδ T cells. *J. Immunol.* 167: 6773–6779.
77. Yamashita, S., Y. Tanaka, M. Harazaki, B. Mikami, and N. Minato. 2003. Recognition mechanism of non-peptide antigens by human γδ T cells. *Int. Immunol.* 15: 1301–1307.
78. Xu, C., H. Zhang, H. Hu, H. He, Z. Wang, Y. Xu, H. Chen, W. Cao, S. Zhang, L. Cui, et al. 2007. γδ T cells recognize tumor cells via CDR3δ region. *Mol. Immunol.* 44: 302–310.